

Cite this: *Energy Environ. Sci.*,
2020, 13, 277

Spherical triboelectric nanogenerator integrated with power management module for harvesting multidirectional water wave energy†

Xi Liang,^{‡,ab} Tao Jiang,^{‡,abc} Guoxu Liu,^{‡,ab} Yawei Feng,^{ab} Chi Zhang^{id} *^{abc} and
Zhong Lin Wang^{id} *^{abcd}

With the increasing deterioration of the natural environment, exploiting clean and renewable energy has become the top priority of scientific research today. One of the most prospective routes is to harvest water wave energy using triboelectric nanogenerator (TENG). In this work, a spherical TENG based on spring-assisted multilayered structure was fabricated to collect multidirectional water wave energy, and a power management module (PMM) was integrated to manage the output energy. The output performance of the TENG device was found to be controlled by the water wave frequency, amplitude, and orientation angle between the triggering direction and middle plane. Furthermore, with the PMM, the spherical TENG could output a steady direct current (DC) voltage on a resistance, and the charging speed to a supercapacitor was improved by 100 times. The power-managed performance of the whole TENG was also influenced by the circuit connection configurations among multilayered TENGs. A digital thermometer and a water level detection/alarm system were successfully driven by the power-managed TENG as the demonstrated applications. This work not only provides a type of spherical TENG capable of harvesting multidirectional water wave energy, but also effectively manages the output energy for practical applications toward blue energy. Our study demonstrates a typical example of how to build a self-charging power pack that can effectively use random energy in a regulated manner.

Received 10th October 2019,
Accepted 22nd November 2019

DOI: 10.1039/c9ee03258d

rsc.li/ees

Broader context

With the deteriorating environment caused by the consumption of traditional energy sources, the exploitation of clean, renewable and sustainable energy sources has become the focus of research. Harvesting ocean wave energy by triboelectric nanogenerators (TENGs) exhibits broad prospects due to their advantages of being lightweight, low fabrication cost and high efficiency. However, the output of previous TENGs is restricted by water wave triggering directions, which is not appropriate for harvesting irregular and random wave energy. Moreover, the large impedance and the unbalanced load matching of TENGs make it difficult for them to power electronic components directly and effectively. In this paper, we not only designed and fabricated a spherical TENG for harvesting water wave energy from multiple triggering directions, but the power management of TENGs was also investigated in detail, demonstrating a typical example of how to build a self-charging power pack that can effectively use random energy in a regulated manner.

Introduction

With the rapid development of the human economy and society, the environment pollution caused by the consumption of fossil fuels imposes a huge challenge to our society. People are becoming gradually conscious of the importance of the research and utilization of clean renewable energy. The ocean occupying 70% of the earth surface contains abundant resources, including water wave energy, which is one of the most promising renewable energy sources for large-scale practical applications.^{1,2} Although it has been explored for decades, the current schemes for collecting water wave energy are still inadequate. That is because of the fact that the commonly adopted electromagnetic generator

^a CAS Center for Excellence in Nanoscience, Beijing Key Laboratory of Micro-nano Energy and Sensor, Beijing Institute of Nanoenergy and Nanosystems, Chinese Academy of Sciences, Beijing 100083, P. R. China. E-mail: zhwang@gatech.edu, czhang@binn.cas.cn

^b School of Nanoscience and Technology, University of Chinese Academy of Sciences, Beijing 100049, P. R. China

^c Center on Nanoenergy Research, School of Physical Science and Technology, Guangxi University, Nanning 530004, China

^d School of Material Science and Engineering Georgia Institute of Technology, Atlanta, GA 30332, USA

† Electronic supplementary information (ESI) available. See DOI: 10.1039/c9ee03258d

‡ These authors contributed equally to this work.

(EMG) is unable to efficiently work under the low frequency of ocean waves.^{3–5}

Triboelectric nanogenerators (TENGs) can effectively harvest mechanical energy to generate electricity from low frequency motions, providing a new approach to capturing water wave energy.^{6–11} Compared with EMGs, TENGs adopt a completely different mechanism, originating from the Maxwell's displacement current.¹² TENGs exhibits obvious advantages such as high power density,^{9,13} high efficiency,^{14–17} light weight,^{18,19} and low fabrication cost, so they can be widely applied for harvesting various energy sources from human motion, to wind and water waves.^{20–28} Among various TENG structures, the spherical TENG is the most representative one for harvesting water wave energy.²⁹ However, the output performance of previously fabricated rolling spherical TENGs is relatively low, greatly limiting the applications.^{30–32} Then we introduced a spring-assisted multilayered structure into a spherical TENG and dramatically optimized the output performance and efficiency.³³ Nevertheless, the as-fabricated spherical TENGs can generate electric energy only at a specific water wave triggering direction due to the restriction of spring orientation, which is not appropriate for harvesting irregular and random wave energy. Therefore, for practical applications, a spherical TENG capable of harvesting water wave energy regardless of the triggering direction is desirable. In addition, the power management of TENGs investigated in our recent work is also worthy of being studied in detail,³⁴ because the large impedance and the unbalanced load matching of TENGs make it difficult for them to power electronic components directly and effectively.^{35,36}

Herein, we designed and fabricated a spherical TENG with a spring-assisted multilayered structure for harvesting water wave energy from multiple triggering directions, and integrated it with a PMM to manage the output energy. First, the output performance of the TENG triggered by water waves with various frequencies and amplitudes was systematically measured, where the influence of the orientation angle reflecting the triggering direction was also addressed. Next, through connecting the PMM with the TENG, the load resistive performance and charging performance were investigated for different circuit connection manners between multilayered TENGs. Finally, the power-managed spherical TENG was applied to power a digital thermometer and drive a water level detection/alarm device, demonstrating the extensive applications of TENGs toward blue energy.

Results and discussion

The structure of the spherical TENG for collecting multi-directional water wave energy, floating on the ocean water surface, is schematically illustrated in Fig. 1a. Such a spherical structure is composed of six multilayered TENGs that are symmetrically located in different directions. Each multilayered TENG has five basic contact-separation mode units as shown in the enlarged view, and there are 30 basic units integrated inside the spherical shell with improved space utilization. A 50 μm -thick

and 4.5 cm-wide Kapton film is shaped in a zigzag structure as the substrate of one multilayered TENG. Each basic TENG unit inside one multilayered TENG consists of a copper electrode and a fluorinated ethylene propylene (FEP) film bonded by another copper electrode. The working mechanism of each basic unit is briefly described in Fig. S1 (ESI[†]). Under the triggering of water waves, the contact and separation of the Cu electrode and FEP film generate opposite charges on their surfaces, and the change of electrical potential difference between two electrodes drives free electrons to flow through the external circuit. For the purpose of increasing the output of each multilayered TENG, four flexible springs adhered to two acrylic blocks are introduced to support the multilayered TENG, which converts the low frequency water wave motions to high frequency vibrations. Six copper balls of 120 g roll and collide with the acrylic substrates attached with the TENGs to make the TENGs work.

The whole spherical structure can be divided into six identical and independent spaces with the acrylic shell as Fig. 1c shows, where the multilayered TENGs working in six different directions do not affect each other. The relative positions of the six spaces inside the spherical shell are also labeled. The fabrication details can be found in the Experimental section. Fig. 1b is the photograph of an as-fabricated spherical TENG device with a diameter of 15 cm. Unlike the previous structures, this spherical TENG is isotropic, so the water wave energy in random directions can be collected without depending on the orientation. In this work, the correlation between the TENG performance and the orientation angle reflecting the triggering direction will be further discussed. Fig. 1d shows a schematic representation for the orientation angle α between the triggering direction of water waves and the middle plane of the spherical TENG. The examples of $\alpha = 60^\circ$ and 45° are presented. The middle plane was defined as the section plane of four internal multilayered TENGs. The triggering direction of water waves is perpendicular to the horizontal plane, because the longitudinal impulse waves were adopted here for conveniently controlling the stable motion of the spherical TENG.

In order to generate the longitudinal impulse waves, a function generator was applied to drive a series of water pumps at the water bottom in the tank. Since the ocean waves in the natural environment have a low frequency below 2.0 Hz, the water wave frequency in the range of 0.5–2.0 Hz was considered in this work. Various amplitudes of water waves can be realized by adjusting the voltage amplitude H_{out} of the function generator. Because of the instability of water waves, it is impossible to accurately measure the wave amplitude or wave height. Therefore, the H_{out} was adopted to reflect the amplitude of water waves, because it is approximately proportional to the water wave amplitude. After sealing and the waterproof process, the spherical TENG was placed in a water tank. Usually, high humidity can greatly reduce the output of TENGs, but the spherical TENG well-sealed by the waterproof tile cement can keep the outputs just with a slight decrease for a long time. When the spherical TENG was triggered by water waves, although the six multilayered TENGs worked in different directions, the basic units in each multilayered TENG were able

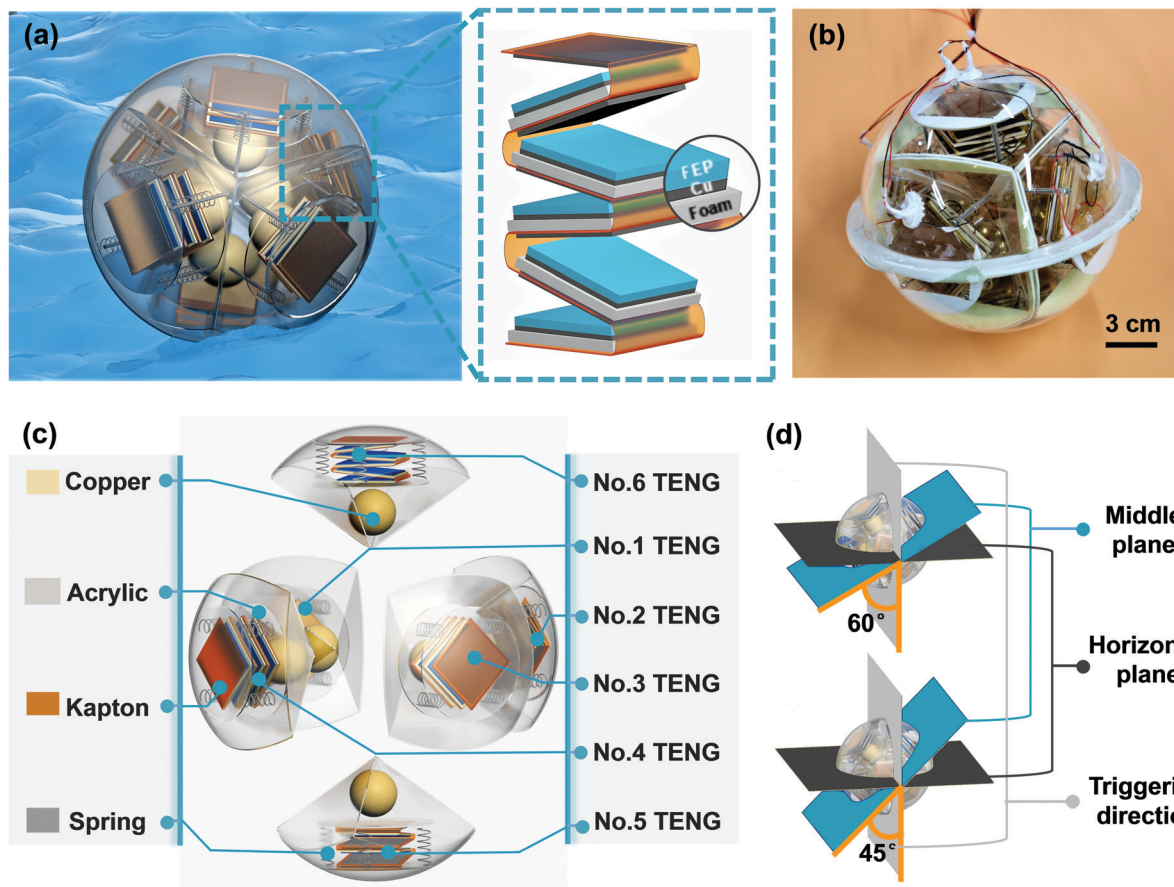


Fig. 1 (a) Schematic diagram of the spherical TENG floating on the ocean water surface, and the enlarged structure of the internal multilayered TENG. (b) Photograph of the as-fabricated spherical TENG device. (c) Exploded view of the spherical TENG. (d) Examples for the orientation angle $\alpha = 60^\circ$ and 45° with the schematic representations of the middle plane, horizontal plane, and triggering direction.

to approximately maintain a synchronous motion. Therefore, the basic units in one multilayered TENG were electrically connected in parallel without rectifier bridges. However, each multilayered TENG was connected with a rectifier bridge before linking with each other for preventing the output counteraction due to the asynchronous motions.

The output performances of each multilayered TENG and the whole spherical TENG were first investigated when the angle α was fixed at 90° , where the middle plane of the spherical TENG coincides with the horizontal plane, and the triggering direction of water waves is perpendicular to the middle plane. Fig. 2a–c shows the output current, transferred charge and output voltage of each multilayered TENG under the water waves with a frequency of 1.0 Hz and $H_{\text{out}} = 2.5$ V. As can be seen, the outputs of the No. 5 TENG are the highest, because the interaction of the copper ball and springs in this space can bring sufficient material surface contact for each basic TENG unit. The output current, transferred charge and the output voltage reached $120 \mu\text{A}$, $1.0 \mu\text{C}$, and 280 V, respectively. As for the No. 1–4 TENGs, the movement directions of the copper balls have an angle with the triggering direction of the water waves, generating lower outputs than the No. 5 TENG. The outputs of the No. 6 TENG are the worst, since the copper ball

located directly below the TENG can only drive the basic TENG units to contact and separate slightly. Then the six TENGs are linked in parallel after separately connecting with rectifier bridges. The typical electrical output performance of the whole spherical TENG under the same water wave conditions is shown in Fig. S2 (ESI†).

Fig. 2d–f presents the rectified output current, voltage and peak power–resistance relationship as the water wave frequency increases from 0.5 Hz to 2.0 Hz at a fixed H_{out} of 2.5 V. It is apparent that the output current and voltage both first increase and then decrease, reaching the maximum values of $200 \mu\text{A}$ and 250 V at a frequency of 1.0 Hz. The output peak power also arrives at the maximum value of 8.5 mW at the frequency of 1.0 Hz and the matched resistance of 1.0 M Ω , and the corresponding power density is 4.81 W m^{-3} according to the device volume. As the water wave frequency increases, the first increase in the output performance is because of the increasing velocity of the copper balls that enhances the pressing force onto the multilayered TENGs. When the frequency is higher than 1.0 Hz, it is easy to make the copper balls oscillate unstably, and the shorter vibration period limits them to sufficiently press the multilayered TENGs. In fact, the optimum frequency is mainly determined by the entire structure consisting

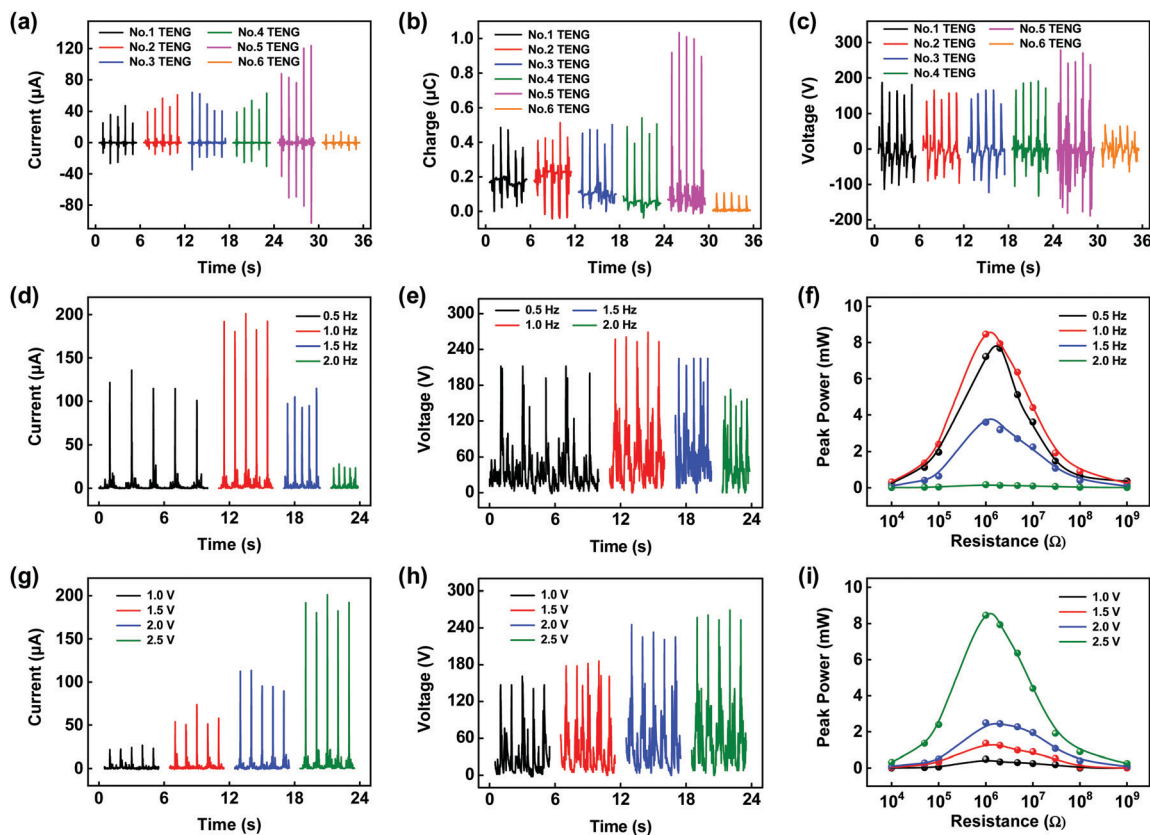


Fig. 2 (a) Output current, (b) transferred charge, and (c) output voltage for each multilayered TENG under the water waves with a frequency of 1.0 Hz and H_{out} of 2.5 V. (d) Rectified output current, (e) output voltage, and (f) output peak power–resistance relationship at various water wave frequencies at fixed H_{out} of 2.5 V. (g) Rectified output current, (h) output voltage, and (i) output peak power–resistance relationship at various water wave amplitudes at fixed frequency of 1.0 Hz.

of copper balls and springs inside the device. Besides the water wave frequency, the influence of the water wave amplitude on the TENG outputs was also studied, as shown in Fig. 2g–i. At the optimal frequency of 1.0 Hz, the output performance of the spherical TENG is positively correlated with the wave amplitude. In other words, larger water wave amplitude is more beneficial to the working of the TENG, and then slight water waves at small wave amplitude cannot fully drive the TENG due to the device weight, leading to a lower output performance.

Subsequently, the influences of the orientation angle α between the water wave triggering direction and the middle plane on the output performance of the spherical TENG were investigated. When the orientation angle changes, the rolling direction of the inner copper balls will be changed, which produces different pressing forces upon the multilayered TENG as triggered by the water waves, leading to varied output performances. The output current, output voltage and peak power–resistance relationship with respect to the angle α are shown in Fig. 3a–c. The angle α varies from 90° to 0° , adopting an optimal water wave frequency of 1.0 Hz and the amplitude H_{out} of 2.5 V. We obtained the output performance at such conditions by addressing the influences of the water wave frequency and amplitude at different angles (Fig. S3 and S4, ESI†). As the angle α increases, the peak values of the output

current and voltage both first decrease and then increase with decreasing angle α , exhibiting the minimum values of $114.5 \mu\text{A}$ and 196 V at an angle α of 45° . The output peak power also has a minimum value of 4.0 mW at $\alpha = 45^\circ$ with a matched resistance of $1 \text{ M}\Omega$. When the angle α is 0° , the output performance is approximately equal to that of $\alpha = 90^\circ$, where the maximum peak power is 8.8 mW . The trend of the output performance related with the angle α is summarized in Fig. 3d. The profiles of current, voltage, and power are centro-symmetric with respect to the angle of $\alpha = 45^\circ$. The reason is that the axis around which the spherical TENG rotates when the angle α changes is an axis of tetragonal symmetry. As a matter of fact, when α arrives at 0° , the spherical TENG returns the same state as $\alpha = 90^\circ$, leading to a similar output performance and constituting a cycle. Moreover, it can be clearly seen that no matter which angle the spherical TENG presents in water waves, the water wave energy conversion can always be realized.

For achieving efficient water wave harvesting and extensive practical applications, a universal and autonomous power management module (PMM) was implemented for the spherical TENG. The circuit schematic diagram of the PMM is demonstrated in the right side of Fig. 4a. The PMM is an AC–DC buck circuit used for the impedance and voltage conversion of the TENG, including a serial switch S , a parallel diode D , a serial

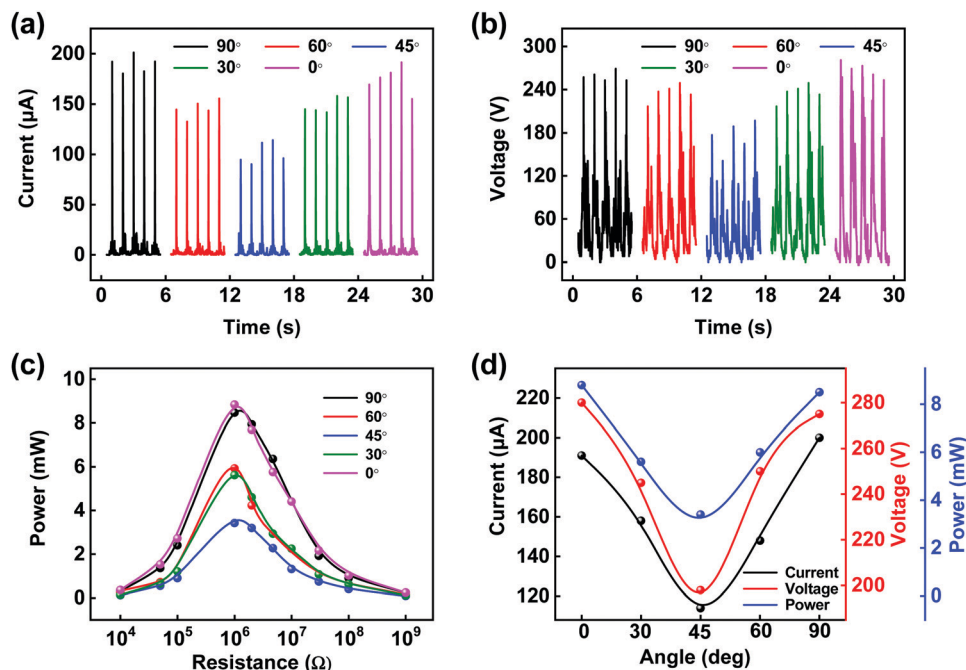


Fig. 3 (a) Output current, (b) output voltage, and (c) output peak power–resistance relationship when the angle α changes from 90° to 0° . (d) Trend of the output performance of the spherical TENG with the decrease of angle α from 90° to 0° .

inductor L (5 mH) and a parallel capacitor C ($10 \mu\text{F}$) in sequence.^{35,36} In the PMM, the state of the switch S is autonomously controlled by the voltage of the TENG with the self-management mechanism, which is realized by a micro-power voltage comparator and a metal–oxide–semiconductor field effect transistor (MOSFET). The detailed circuit layout of the power management module and its top-view photograph after packaging are shown in Fig. S5 (ESI[†]). A comparison of the charging voltage between the direct charging and managed charging processes for charging a supercapacitor of 0.1 F was made, as shown in Fig. 4b. The water wave frequency was fixed as 1.0 Hz and the amplitude H_{out} was 2.5 V. Through direct charging for 360 s, the voltage on the capacitor hardly rises. However, the voltage increases from 0 to 0.64 V in the PMM with 100 times improvement in the stored energy (inset of Fig. 4b). With the strategy of maximized energy transfer, the autonomous and sequential switching of the MOSFET inside the PMM corresponds with the previous studies using a parallel switch to achieve maximized energy output cycle (CMEO). Therefore, the PMM can maximally extract electrical energy from the TENG and transfer it to the back-end capacitors, significantly improving the charging speed and stored energy.³⁶ In addition, through the PMM, random and irregular electrical outputs can be converted into a steady DC voltage, meeting the voltage demands of common electronics.

Integrated with the PMM, we investigated the electrical outputs of the power-managed spherical TENG with various circuit connection manners between six multilayered TENGs under the water waves. The schematic diagram for the parallel and series connections is presented in Fig. 4a. The switch S in the PMM has a threshold voltage. If the threshold voltage is set as a high value that the TENGs in series connection can reach

always, but the TENGs in parallel can reach occasionally, the output voltage of the PMM-integrated spherical TENG will have a faster increase for the series connection, as shown in Fig. S6 (ESI[†]). The series connection is conducive to the working of the PMM at this time. In the next studies, we are focused on the case that the threshold voltage of the switch S is lower than that of both the TENGs in series and in parallel. The output voltage on a load resistance produced by the power-managed spherical TENG with the internal TENGs connected in parallel and in series was measured, as shown in Fig. 4c and d. All the voltage curves first rise rapidly in a short time and then reach steady states. The steady and continuous DC output voltage is realized on the resistor, because the switch in the PMM is not only used for the maximized energy transfer but also for DC buck conversion in the circuit, and the LC unit in the circuit plays a role of low pass filter, which retains the DC component and restrains the high frequency harmonic component in output voltage.³⁶ The stable DC voltage values at different resistances are extracted in Fig. 4e, showing that the saturated voltage increases with increasing resistance. Furthermore, the voltage for the parallel connection manner increases from 0.31 V to 10.5 V as the resistance varies from 10 k Ω to 1 G Ω , while the voltage for the series manner only increases from 0.22 V to 8.5 V. In this case where both the TENGs in two connection manners can always reach the threshold voltage, the time periods of the switch in the PMM turned on are nearly the same, so that the higher current provided by TENGs in parallel connection can realize a higher output voltage and translated energy.

Then the charging performance of the spherical TENG with the PMM to load capacitors was also compared for the parallel

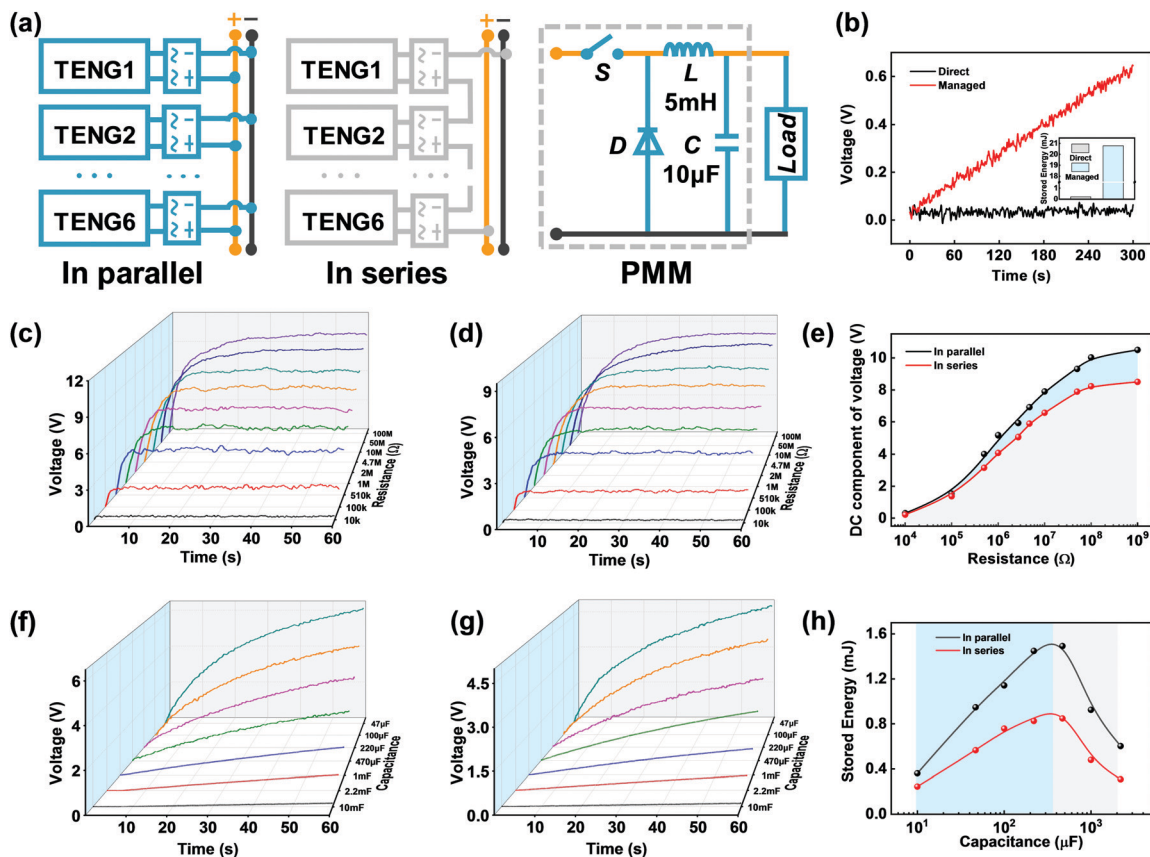


Fig. 4 (a) Schematic diagrams for the parallel and series connections between the multilayered TENG units inside the spherical TENG, and the circuit schematic diagram of the PMM. (b) Comparison of the charging voltage and stored energy between the direct charging and managed charging for charging a supercapacitor of 0.1 F under the water waves at a frequency of 1.0 Hz and amplitude H_{out} of 2.5 V. (c and d) Output voltage on a load resistance produced by the power-managed spherical TENG with the parallel and series connections, respectively. (e) Saturated DC voltage values with respect to the load resistance. (f and g) Charging voltage on various load capacitors for the spherical TENG with the parallel and series connections. (h) Stored energy with the capacitance increasing from 47 μF to 10 mF for the two connection manners.

and series connections. As shown in Fig. 4f and g, for each capacitance, the charging voltage first increases at a faster speed, and then increases until saturated with a decreasing charging speed. The charging speed for a smaller capacitance is faster, and a higher charging voltage can be achieved during the charging time of 60 s. We can also view that the charging voltage for the parallel connection is higher. Fig. 4h characterizes the stored energy with the capacitance from 47 μF to 10 mF for two connection manners. For the TENGs in parallel connection, the stored energy gets a maximum value of 1.6 mJ at the capacitance of 470 μF . While the maximum stored energy for the series connection is only 0.8 mJ, although the matched capacitance under the two circuit connections is identical. Therefore, the parallel connection is also more beneficial for the energy storage, as well as the energy conversion.

Finally, the applications of the power-managed spherical TENG for harvesting water wave energy were demonstrated. The conception of utilizing the spherical TENG integrated with the PMM to realize detection, display and alarm for marine information including water temperature and water level is illustrated in Fig. 5a. Here, we chose a digital thermometer and a water level detection/alarm device to achieve the idea under

laboratory conditions. The internal multilayered TENGs in the spherical device were connected in parallel, and the water wave conditions with a frequency of 1.0 Hz and amplitude H_{out} of 2.5 V were adopted. Fig. 5b is the voltage profile on the thermometer powered by the spherical TENG integrated with the PMM. The voltage on the thermometer can rapidly rise to 1.3 V within the charging time of 2 s, and the thermometer starts to measure the water temperature and display the value. Next, the thermometer is able to work constantly, since the voltage value continues to fluctuate between 1.3 V to 2.0 V as long as the water waves are generated. The photograph of lighting up the liquid crystal display (LCD) screen of the thermometer is presented in the inset. The experimental process is recorded in Movie S1 (ESI[†]).

Besides the digital thermometer, the application of driving a water level detection/alarm device was also shown, as in Fig. 5c. The design of the device introduces five level float switches aligned from low to high in a water tank for autonomous control, containing three normally-off switches marked by S1, S3 and S5 and two normally-on switches of S2 and S4. Above all, the S1 and S2 are linked in series to control an LCD and a light emitting diode (LED) simplified as L1 in Fig. 5c. The S3 and S4

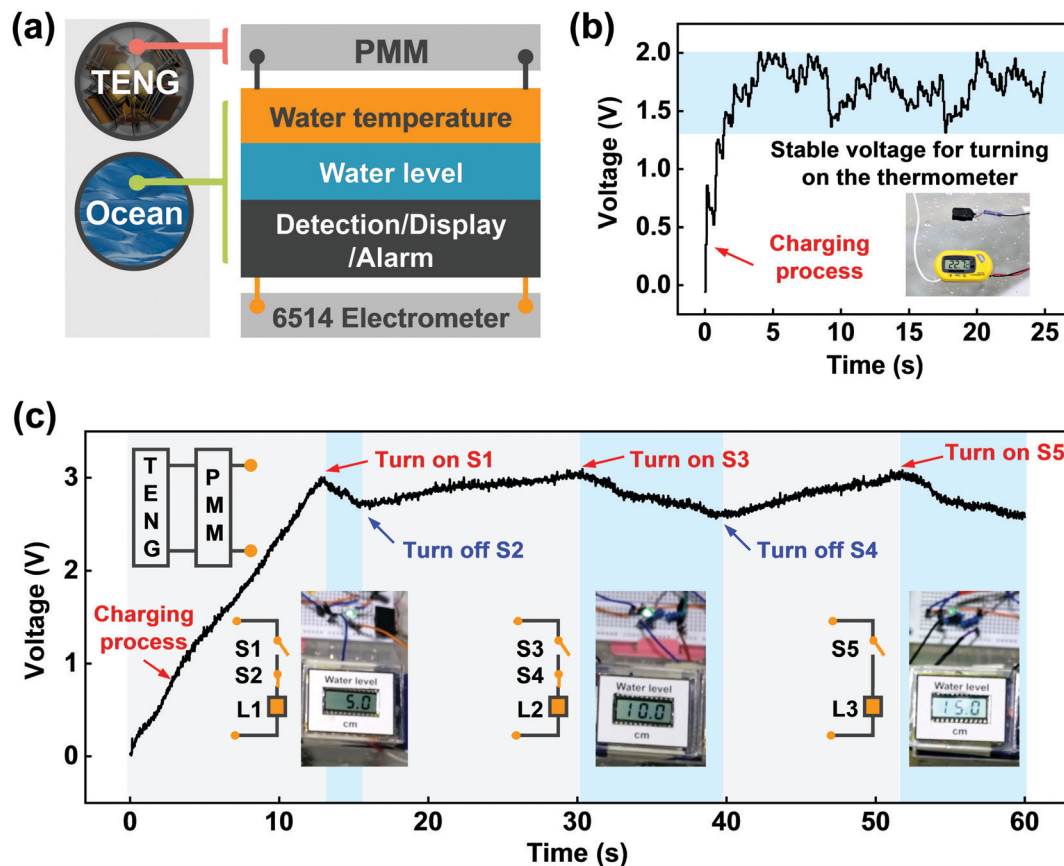


Fig. 5 (a) Framework for the integrated self-powered marine information detection/display/alarm system driven by the power-managed spherical TENG. (b) Application demonstration for powering a digital thermometer. The voltage profile on the thermometer and the photograph of the PMM and the LCD screen are shown. (c) Application demonstration for driving a water level detection/alarm device. The voltage on the detection/alarm device, schematic connection between the switches and the device, and photographs of the LCD display for water level detection and the LED lit-up as an alarm are shown.

in series are employed to control L2 accordingly, while S5 is the switch of L3. Afterward, the three parts are connected in parallel and driven by the power-managed spherical TENG. The charging process takes 13 s before the water level rises to 5 cm, and the voltage varies from 0 to 3 V. When the water level reaches 5 cm, the normally-off switch S1 is submerged to be turned on. As a result, LED 1 is lit-up to give an alarm, and the LCD 1 displays the value of the water level. After the water level rises a little more, the L1 is extinguished, because the normally-on switch S2 is submerged to be turned off. The working principles of lighting up L2 and L3 when the water level respectively reaches 10 cm and 15 cm are similar. The experimental process is shown in Movie S2 (ESI[†]). By continuous water waves, this device can autonomously measure the water level and provide an LCD display and alarm, which is of great significance for marine warning.

Conclusions

In summary, we designed and fabricated a spherical TENG device by integrating six spring-assisted multilayered TENGs for

harvesting multidirectional water wave energy and then integrated it with the PMM. The influences of water wave frequency and amplitude on the output performance were investigated, showing that the maximum outputs of 80 μ A, 250 V, and 8.5 mW were obtained at the orientation angle of 90° under the wave conditions of 1.0 Hz and H_{out} of 2.5 V. Then the output performance of the spherical TENG with respect to the orientation angle was studied, proving that the energy conversion could always be achieved regardless of the angle reflecting the triggering direction. Furthermore, by integrating with the PMM, a steady and continuous DC voltage can be generated on the load resistor, and the stored energy could be greatly improved by 100 times for charging a supercapacitor of 0.1 F. The circuit connection manner between internal TENGs in the spherical device was also found to affect the power-managed output voltage. Finally, a digital thermometer and a water level detection/alarm device were successfully driven by the power-managed spherical TENG, demonstrating the broad application prospects toward large-scale blue energy harvesting. Our study demonstrates a typical example of how to build a self-charging power pack that can effectively use random energy in a regulated manner, which is the future of battery technologies for the internet of things.

Experimental

Fabrication of the spherical TENG device

First, we divided the acrylic spherical shell with a diameter of 15 cm into six identical spaces by eight fan-shaped acrylic sheets of suitable sizes. Second, we fabricated the multilayered TENGs inside the spherical TENG. A Kapton strip (27 cm × 4.5 cm) was divided equally into six squares and then shaped into a zigzag structure, which was used as the substrate of the multilayered TENG. Copper foils (4 cm × 4 cm) and FEP films (4 cm × 4 cm) bonded with other copper foils were alternately adhered on both sides of the Kapton strip, forming five basic TENG units. The Cu side of each FEP-Cu film was attached to a foam block (4.5 cm × 4.5 cm × 1 mm) to achieve sufficient contact and separation of the triboelectric materials. For the tribo-materials (FEP), we injected electrons onto their surfaces through corona discharge technology at 5 kV for 5 min. After that, the five polarized TENG units were directly linked in parallel. Next, two circular acrylic sheets with a diameter of 7 cm and a thickness of 1 mm were applied to sandwich the multilayered TENG. Four flexible springs with a length of 4 cm placed over screws were stuck between the two acrylic sheets to support the structure. After repeating this structure to six copies, they were separately placed in the six spaces of the acrylic spherical shell together with six copper balls (120 g), composing the spherical TENG that can harvest water wave energy in various directions. Finally, we sealed and waterproofed the spherical TENG using the tile cement for working in the water environment.

Electric measurements of the TENG device

The water waves applied in this work were generated by a series of wave pumps (rw-20 JEPOWER TECHNOLOGY Inc.) and controlled by a function generator (AFG3011C Tektronix Inc.). The output current and transferred charge of the spherical TENG and the voltage managed by the PMM were measured by a current preamplifier (Keithley 6514 System Electrometer), while the output voltage directly produced by the TENGs was measured by a digital oscilloscope (Agilent InfiniiVision 2000X).

Conflicts of interest

The authors declare no competing financial interest.

Acknowledgements

Support from the National Key R&D Project from Minister of Science and Technology (2016YFA0202704), National Natural Science Foundation of China (Grant No. 51432005 and 51702018) and Beijing Natural Science Foundation (No. 4192070) is appreciated. The authors also thank Kai Han, Jie An, and Xiaodan Yang for device fabrication and measurements.

Notes and references

- 1 S. P. Beeby, R. N. Torah, M. J. Tudor, P. Glynne-Jones, T. O'Donnell, C. R. Saha and S. Roy, *J. Micromech. Microeng.*, 2007, **17**, 1257–1265.

- 2 Z. L. Wang, T. Jiang and L. Xu, *Nano Energy*, 2017, **39**, 9–23.
- 3 X. Wang and Y. Yang, *Nano Energy*, 2017, **32**, 36–41.
- 4 Z. Wu, H. Guo, W. Ding, Y. C. Wang, L. Zhang and Z. L. Wang, *ACS Nano*, 2019, **13**, 2349–2356.
- 5 J. Wang, L. Pan, H. Guo, B. Zhang, R. Zhang, Z. Wu, C. Wu, L. Yang, R. Liao and Z. L. Wang, *Adv. Energy Mater.*, 2019, **9**, 1802892.
- 6 Y. Y. Yao, T. Jiang, L. M. Zhang, X. Y. Chen, Z. L. Gao and Z. L. Wang, *ACS Appl. Mater. Interfaces*, 2016, **8**, 21398–21406.
- 7 L. Xu, T. Jiang, P. Lin, J. J. Shao, C. He, W. Zhong, X. Y. Chen and Z. L. Wang, *ACS Nano*, 2018, **12**, 1849–1858.
- 8 J. Wang, Z. Wu, L. Pan, R. Gao, B. Zhang, L. Yang, H. Guo, R. Liao and Z. L. Wang, *ACS Nano*, 2019, **13**, 2587–2598.
- 9 M. Xu, T. Zhao, C. Wang, S. L. Zhang, Z. Li, X. Pan and Z. L. Wang, *ACS Nano*, 2019, **13**, 1932–1939.
- 10 X. J. Zhao, S. Y. Kuang, Z. L. Wang and G. Zhu, *ACS Nano*, 2018, **12**, 4280–4285.
- 11 Z. L. Wang, *Faraday Discuss.*, 2014, **176**, 447–458.
- 12 Z. L. Wang, *Mater. Today*, 2017, **20**, 74–82.
- 13 G. Cheng, H. Zheng, F. Yang, L. Zhao, M. Zheng, J. Yang, H. Qin, Z. Du and Z. L. Wang, *Nano Energy*, 2018, **44**, 208–216.
- 14 L. Xu, Y. K. Pang, C. Zhang, T. Jiang, X. Y. Chen, J. J. Luo, W. Tang, X. Cao and Z. L. Wang, *Nano Energy*, 2017, **31**, 351–358.
- 15 P. Cheng, H. Guo, Z. Wen, C. Zhang, X. Yin, X. Li, D. Liu, W. Song, X. Sun, J. Wang and Z. L. Wang, *Nano Energy*, 2019, **57**, 432–439.
- 16 W. Tang, T. Jiang, F. R. Fan, A. F. Yu, C. Zhang, X. Cao and Z. L. Wang, *Adv. Funct. Mater.*, 2015, **25**, 3718–3725.
- 17 H. S. Wang, C. k. Jeong, M. H. Seo, D. J. Joe, J. H. Han, J. B. Yoon and K. J. Lee, *Nano Energy*, 2017, **35**, 415–423.
- 18 F. R. Fan, Z. Q. Tian and Z. L. Wang, *Nano Energy*, 2012, **1**, 328–334.
- 19 G. Zhu, Y. S. Zhou, P. Bai, X. S. Meng, Q. S. Jing, J. Chen and Z. L. Wang, *Adv. Mater.*, 2014, **26**, 3788–3796.
- 20 T. Jiang, X. Y. Chen, C. B. Han, W. Tang and Z. L. Wang, *Adv. Funct. Mater.*, 2015, **25**, 2928–2938.
- 21 Z. R. Liu, J. H. Nie, B. Miao, J. D. Li, Y. B. Cui, S. Wang, X. D. Zhang, G. R. Zhao, Y. B. Deng, Y. H. Wu, Z. Li, L. L. Li and Z. L. Wang, *Adv. Mater.*, 2019, **31**, 1807795.
- 22 X. Yang, L. Xu, P. Lin, W. Zhong, Y. Bai, J. Luo, J. Chen and Z. L. Wang, *Nano Energy*, 2019, **60**, 404–412.
- 23 L. M. Zhang, C. B. Han, T. Jiang, T. Zhou, X. H. Li, C. Zhang and Z. L. Wang, *Nano Energy*, 2016, **22**, 87–94.
- 24 K. W. Lim, M. Peddigari, C. H. park, H. Y. Lee, Y. Min, J. W. Kim, C. W. Ahn, J. J. Choi, B. D. Hagn, J. H. Choi, D. S. Park, J. K. Hong, J. T. Yeom, W. H. Yoon, J. Ryu, S. N. Yi and G. T. Hwang, *Energy Environ. Sci.*, 2019, **12**, 666–674.
- 25 B. S. Zhang, Y. J. Tang, R. R. Dai, H. Y. Wang, X. P. Sun, C. Qin, Z. F. Pan, E. J. Liang and Y. C. Mao, *Nano Energy*, 2019, **64**, 103953.
- 26 M. Wang, J. H. Zhang, Y. J. Tang, J. Li, B. S. Zhang, E. J. Liang, Y. C. Mao and X. D. Wang, *ACS Nano*, 2018, **12**, 6156–6162.

- 27 C. Ning, L. Tian, X. Y. Zhao, S. X. Xiang, Y. J. Tang, E. J. Liang and Y. C. Mao, *J. Mater. Chem. A*, 2018, **6**, 19143–19150.
- 28 M. Wang, N. Zhang, Y. J. Tang, H. Zhang, C. Ning, L. Tian, W. H. Li, J. H. Zhang, Y. C. Mao and E. J. Liang, *J. Mater. Chem. A*, 2017, **5**, 12252–12257.
- 29 X. F. Wang, S. M. Niu, Y. J. Yin, F. Yi, Z. You and Z. L. Wang, *Adv. Energy Mater.*, 2015, **5**, 1501467.
- 30 T. X. Xiao, T. Jiang, J. X. Zhu, X. Liang, L. Xu, J. J. Shao, C. L. Zhang, J. Wang and Z. L. Wang, *ACS Appl. Mater. Interfaces*, 2018, **10**, 3616–3623.
- 31 T. Jiang, Y. Y. Yao, L. Xu, L. M. Zhang, T. X. Xiao and Z. L. Wang, *Nano Energy*, 2017, **31**, 560–567.
- 32 T. Jiang, L. M. Zhang, X. Y. Chen, C. B. Han, W. Tang, C. Zhang, L. Xu and Z. L. Wang, *ACS Nano*, 2015, **9**, 12562–12572.
- 33 T. X. Xiao, X. Liang, T. Jiang, L. Xu, J. J. Shao, J. H. Nie, Y. Bai, W. Zhong and Z. L. Wang, *Adv. Funct. Mater.*, 2018, **28**, 1802634.
- 34 X. Liang, T. Jiang, G. Liu, T. Xiao, L. Xu, W. Li, F. Xi, C. Zhang and Z. L. Wang, *Adv. Funct. Mater.*, 2019, 1807241.
- 35 F. Xi, Y. Pang, G. Liu, S. Wang, W. Li, C. Zhang and Z. L. Wang, *Nano Energy*, 2019, **61**, 1–9.
- 36 F. B. Xi, Y. K. Pang, W. Li, T. Jiang, L. M. Zhang, T. Guo, G. X. Liu, C. Zhang and Z. L. Wang, *Nano Energy*, 2017, **37**, 168–176.